J. Membrane Biol. 194, 11–20 (2003)
DOI: 10.1007/s00232-003-2022-z

The Journal of
Membrane
Biology

The Gating Kinetics of the Slow Vacuolar Channel. A Novel Mechanism for SV Channel Functioning?

H. Miedema[1], **A.H. de Boer**[2], **O. Pantoja**[3]
[1]Facultad de Ciencias, UAEM, Av. Universidad 1001, Cuernavaca, Morelos 62210, Mexico
[2]BioCentrum Amsterdam, Department of Developmental Genetics, Faculty of Biology, Vrije Universiteit, De Boelelaan 1087, 1091 HV Amsterdam, The Netherlands
[3]Departamento de Biología Molecular de Plantas, Instituto de Biotecnología, UNAM, Cuernavaca, Morelos 62250, Mexico

Received: 15 October 2002/Revised: 22 February 2003

Abstract. Although there is consensus that the slow vacuolar or SV channel is a Ca^{2+} release channel, the underlying mechanism of operation is still controversial. The main reason is that the voltage sensitivity of SV gating seems to exclude activation at hyperpolarized (physiological) membrane potentials. Inspired by a study of Gambale et al. (1993) and supported by simulation studies presented here, we interpreted SV activation and deactivation kinetics in terms of a cyclic state diagram originally applied to animal cation-selective channels. A cyclic state diagram allows two pathways of activation operating in opposite directions. One pathway represents the frequently observed slow activation at moderate depolarization (<130 mV). With the open state (O) next to the closed state initially occupied (C_1), direct transitions from C_1 to O can account for the fast activation observed at higher depolarized potentials (>130 mV). We hypothesize that similar state transitions directly to O may also occur during hyperpolarization. The implication of this proposed mechanism is that SV accomplishes its physiological role during hyperpolarization-evoked deactivation. Despite their rare occurrence and possibly short duration, these opening events may last long enough to substantially raise the local cytosolic free Ca^{2+} level at the channel mouth by as much as 600 nM/ms. Because under in vivo conditions the Ca^{2+} flux is inwardly directed, the mechanism presented here revives the notion that the SV channel can be subject to calcium-induced calcium release.

Key words: SV channel — State diagram — Gating kinetics — Ca^{2+} release — Plant vacuole

Introduction

In contrast to animal cells, plant cells contain a central vacuole that can occupy up to 90 percent of the cell's volume. The vacuole plays a key role in turgor and solute compartmentalization. By virtue of its size, the vacuole is the most prominent sink for Ca^{2+} (Sanders, Brownlee & Harper, 1999). Several distinct Ca^{2+}-permeable ion channels have been identified in the vacuolar membrane (Johannes, Brosnan & Sanders, 1992). Of the different types of ion channels present in the tonoplast, the slow-activating vacuolar or SV channel has been characterized in most detail. The SV channel is ubiquitous and has been identified in all green plant species studied so far. These studies show that the SV channel is regulated not only by membrane voltage and cytosolic Ca^{2+}, as reported in the seminal study by Hedrich and Neher (1987), but in addition by redox potential (Carpaneto, Cantù & Gambale, 1999) and a plethora of other cell physiological parameters (Allen & Sanders, 1997). Because the SV channel shows permeability towards Ca^{2+}, it was suggested that the channel is involved in the Ca^{2+} homeostasis of the cell (Pantoja, Gelli & Blumwald, 1992). Considering the eminent role of the cytosolic free Ca^{2+} level (Ca_{cyt}), this could indeed explain why the channel is regulated at so many different levels.

Despite the vast amount of knowledge about the regulation of the SV channel, there are still controversies around its physiological role. Two questions dominate the debate on SV functioning. First, given the Ca^{2+} permeability and its activation by Ca_{cyt}, can the gating kinetics of SV account for calcium-induced

Correspndence to: H. Miedema; email: miedema@biomade.ne
Present address for H. M.: BioMade Technology Foundation, Nijenborgh 4, 9747 AG Groningen, The Netherlands

calcium release (CICR) out of the vacuole, a mechanism originally proposed by Ward and Schroeder (1994)? Pottosin et al. (1997) quantified the Ca^{2+}- and voltage-dependent gating of SV and concluded that the SV channel cannot be involved in CICR. Here we focus on the second question that concerns the voltage sensitivity of the SV channel in relation to the trans-tonoplast potential under in vivo conditions. Referenced to the cytosol, the trans-tonoplast potential (V_m) is in the range of −50 to 0 mV. The opening and closing (gating) of the SV channel is sensitive to V_m, consequently, the physiological role of SV hinges on the voltage range the channel is activated. Figure 2*B* summarizes and highlights the motivation of the present study. Under in vitro patch-clamp conditions, the SV channel is activated at positive, i.e., non-physiological V_m, while under in vivo conditions with V_m in the range of −50 to 0 mV, the SV channel is virtually completely deactivated. Apart from the cytosolic Mg^{2+} level (but *see* Discussion), parameters that are able to shift the activation potential of SV into the range of physiological V_m have not been identified so far (Pottosin et al., 1997). We thus face a striking paradox; on the one hand, the SV channel is a multilevel regulated transport protein but, on the other hand, the prevailing V_m prevents activation under in vivo conditions. Compared to the study of regulatory mechanisms much less attention has been paid to the precise kinetics of SV channel activation and deactivation. With the study of Gambale et al. (1993) as a starting point, the aim of the present study was to shed some light on the gating kinetics of the SV channel and identify a mechanism that allows SV to perform its physiological role. The possibility of CIRC is re-evaluated in the context of the SV gating properties presented here.

Materials and Methods

Plant Material

Mesembryanthemum crystallinum L. was grown as described by Barkla et al. (1999). A detailed protocol for the isolation of leaf mesophyll protoplasts can be found elsewhere (Miedema, Balderas & Pantoja, 2000). Briefly, after stripping off the epidermis at the abaxial side, leaf segments were incubated for 45 min at 30°C in an enzyme solution containing 0.05% cellulase RS (Onozuka, Japan), 0.01% pectolyase Y-23 (Seishin, Japan) and 1% BSA (Sigma, Mexico). In order to obtain vacuoles, 0.9 ml of a 100 mM EGTA solution (adjusted with Tris to pH 7, resulting in a final osmolarity of 200 mM) was added to 0.3 ml of protoplast solution. Protoplast lysis was stopped by the addition of 10 ml bath solution. All experiments were performed at room temperature (19–21°C).

Patch Clamp

Patch-clamp recording and data analysis were performed with an Axopatch 200B amplifier, a 1200 Digidata interface and pClamp 6.0.4 software (Axon Instruments, Foster City, CA). Whole-vacuole data were sampled at 2 kHz and filtered at a −3 dB frequency of 1 kHz using the electronics on the Axopatch amplifier. Pipettes were pulled from glass capillaries (Sigma, Mexico, # P-1174), using a two-stage pipette puller (Narishige, Tokyo, # PP-83).

The solutions used contained K_2Malate, as specified in the legend of each figure. The pipette solution contained 10 mM MES, pH 5.5 and the bath solution 10 mM HEPES, pH 7.5. All solutions also contained $CaCl_2$, resulting in a free Ca^{2+} activity of 0.3 mM. Malate was added as malic acid and the pH of the solutions was adjusted with KOH. Sorbitol was added to all solutions to a final osmolality of 500 mM. Ion activities were calculated according to Robinson and Stokes (1965). A 2.5 M KCl/2% agar bridge connected the reference electrode to the bath solution. Following the current and voltage convention for endomembranes proposed by Bertl et al. (1992) implies that, when recording in the whole-vacuole or outside-out patch configuration, a flux of cations into the vacuole is assigned as an outward, positive current. Likewise, the membrane potential (V_m) equals the negative of the applied pipette potential (V_p). Throughout the text, membrane potentials have been corrected for liquid junction potentials (Ward & Schroeder, 1994; Miedema & Pantoja, 2001).

With a series resistance (R_s) of 10 MΩ (with 100 mM K_2Malate in the pipette) and a maximal current magnitude of 1 nA, as recorded in outside-out macro patches, the voltage drop across R_s was 10 mV at most. We therefore did not correct the data of Fig. 2*B*; moreover, the degree of activation is expressed as the ratio of two current magnitudes, which further diminishes the R_s effect.

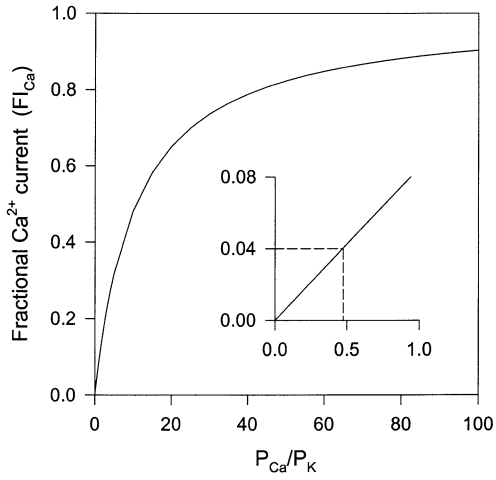

Fig. 1. The fractional Ca^{2+} current (FI_{Ca}) in relation to P_{Ca}/P_K. The fractional Ca^{2+} current was calculated according to Eq. 1, while assuming Ca_{vac} = 2 mM, Ca_{cyt} = 100 nM, K_{vac} = 100 mM, K_{cyt} = 100 mM and V_m = −25 mV. These ionic conditions are based on the values listed by Allen and Sanders (1997). The inset shows the same data but on an enlarged scale for small values of P_{Ca}/P_K.

Calculation of the Fractional Ca^{2+} Current through SV

The SV channel is permeable to monovalent and divalent cations. In the presence of the two permeable ion species K^+ and Ca^{2+}, the fraction of current that is actually carried by Ca^{2+} is defined as $I_{Ca}/(I_K + I_{Ca})$ (*see* Schneggenburger, Zhou & Neher, 1993). An expression of the fractional Ca^{2+} current (FI_{Ca}) can readily be derived from the Goldman-Hodgkin-Katz (*GHK*)-current equation and is given by:

$$FI_{Ca} = \frac{I_{Ca}}{I_{Ca} + I_K} = \frac{1}{1 + \frac{(K_{cyt} - \alpha K_{vac})(1-\beta)}{\gamma(Ca_{cyt} - \beta Ca_{vac})(1-\alpha)}} \quad (1)$$

where α represents $\exp(-V_m F/RT)$, β is $\exp(-2V_m F/RT)$, γ equals $4P_{Ca}/P_K$ and RT/F is 25.3 mV at 20°C. Figure 1 shows the relationship between P_{Ca}/P_K and FI_{Ca}, calculated for prevailing physiological conditions.

Simulations of SV Gating Kinetics

All simulations were performed using the next set of differential equations, derived from the laws of mass action and describing the transitions between neighboring states in Fig. 8*A*.

$$dC_1/dt = k_2C_2 + k_{12}C_5 + k_9O - (k_1 + k_{10} + k_{11})C_1$$

$$dC_2/dt = k_1C_1 + k_4C_3 + k_{15}C_5 - (k_2 + k_3 + k_{16})C_2$$

$$dC_3/dt = k_3C_2 + k_6C_4 - (k_4 + k_5)C_3$$

$$dC_4/dt = k_5C_3 + k_8O - (k_6 + k_7)C_4$$

$$dC_5/dt = k_{11}C_1 + k_{16}C_2 + k_{14}C_6 - (k_{12} + k_{13} + k_{15})C_5$$

$$dC_6/dt = k_{13}C_5 - k_{14}C_6$$

$$dO/dt = k_{10}C_1 + k_7C_4 - (k_8 + k_9)O$$

Simulations were performed with Power Law Analysis and Simulation software (PLAS; A. E. N. Ferreira, 1996–2000, *see* Voit, 2000), using a step size of 0.01 s. Although originally designed for the analysis of biochemical pathways (Voit, 2000), the PLAS software served us extremely well in simulating ion channel (de) activation kinetics.

Results

Figure 2*A* shows the activation kinetics of SV current recorded on an excised outside-out macro patch upon pulsing from a holding potential (HP) of 0 mV to depolarized V_m ranging from −30 to 150 mV, in 10 mV steps. Sigmoid or S-shaped current activation as shown in Fig. 2*A*, indicates the existence of several nonconducting or closed states. The least complex gating diagram of SV, as shown in Fig. 3*A*, thus comprises several of these closed states (*C*) and one conducting or open state (*O*). Such a kinetic scheme is also in accordance with the observed effect of HP on the activation kinetics. Figure 4 shows time courses of whole-vacuole current activation after pulsing from either a HP of −60 (trace #*1*) or 0 mV (trace #*2*) to 120 mV. At −60 mV, more channels are forced into closed states farther removed from the open state. As a result, when pulsing from a HP of −60 mV, more state transitions are required to reach the open state and this is reflected in a slower activation.

With pulses to more depolarized V_m (>130 mV), the activation kinetics changed and an example is shown in Fig. 5*A*. After a fast activation, the current started to partly deactivate. Similar shoulders in the activation of SV have been observed previously (Miedema et al., 2000), as well as in other preparations (Gambale et al., 1993; Pottosin et al., 1997; Van den Wijngaard et al., 2001). The appearance of a shoulder during activation can be explained by the presence of an additional closed state next to the open state as shown in the state diagram of Fig. 3*B*. Assume that at the start of the activating voltage pulse most of the channels occupy state C_1. Upon activation, transitions start to occur from C_1 to C_n and eventually to *O*. But when time progresses,

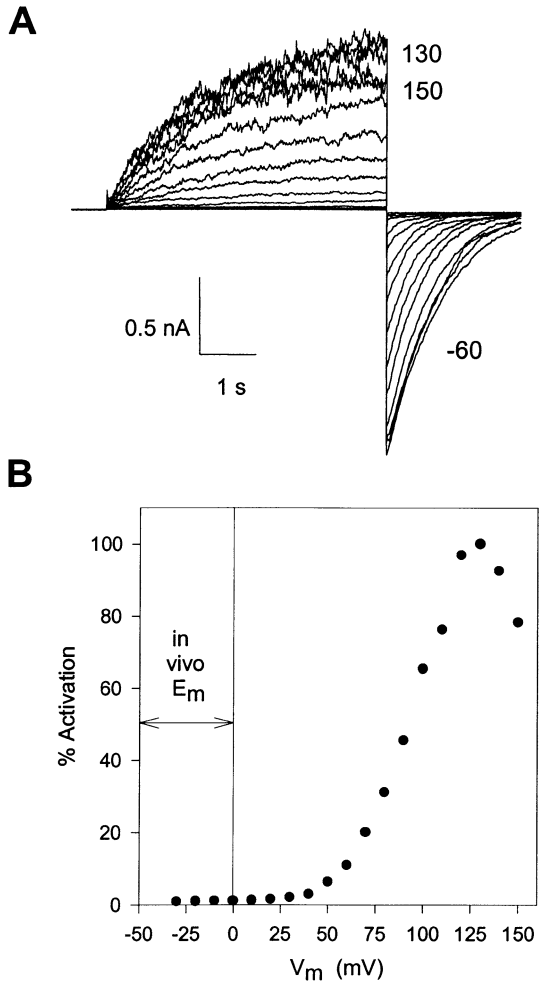

Fig. 2. Voltage dependence of SV current activation. (*A*) Voltage-clamp current recordings on an outside-out macro patch of a *M. crystallinum* vacuole in symmetrical 10 mM K_2Malate solutions. The membrane potential (V_m) was stepped from a holding potential of 0 mV to potentials ranging from −30 mV to 150 mV, in 10-mV steps, followed by a deactivating pulse of −60 mV. Note the decline of current magnitude at high depolarized potentials (>130 mV). (*B*) The degree of activation as a function of V_m, obtained from the recording shown in (*A*). The degree of activation was defined as the steady-state current magnitude measured at the end of the voltage pulse relative to the steady-state peak current recorded at 130 mV.

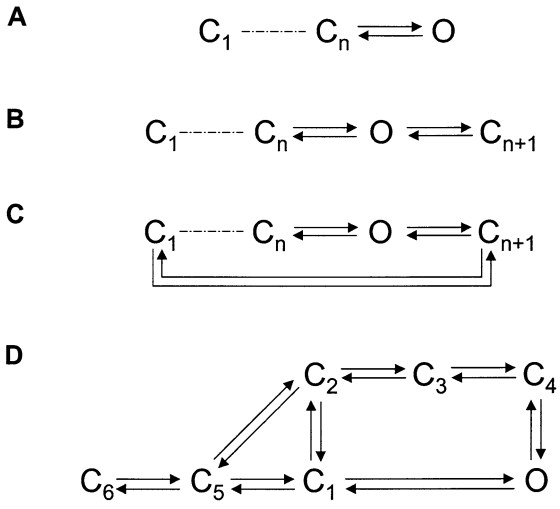

Fig. 3. Minimal gating state diagrams of the SV channel. (*A*) Linear state diagram consisting of n non-conducting or closed states (C_1 to C_n) and one conducting or open state (O). (*B*) The diagram of (*A*) extended with an additional closed state (C_{n+1}), resulting in an open state in between two closed states. (*C*) The diagram of (*B*) while allowing direct transitions between C_1 and C_{n+1}. (*D*) Minimal state diagram of a number of cation-selective channels in animal cells (*see* text). It should be noted, however, that states C_2, C_3 and C_4 of animal ion channels represent inactivated rather than closed states.

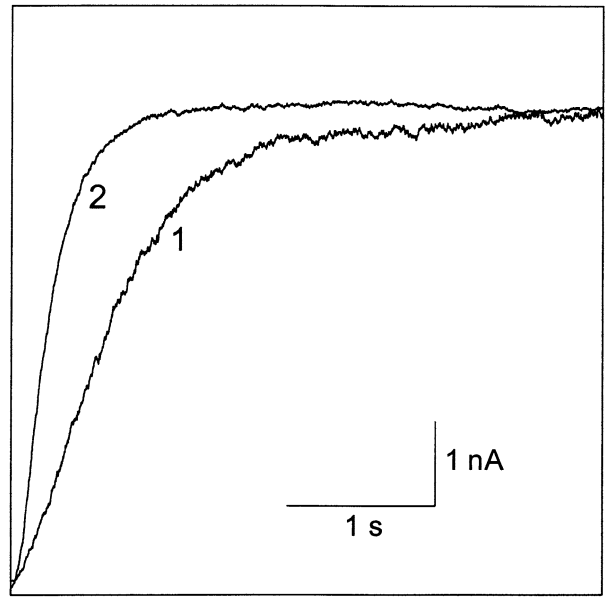

Fig. 4. Effect of the holding potential on SV activation kinetics. Whole-vacuole recordings in symmetrical 10 mM K_2Malate solutions after pulsing from a holding potential of either −60 mV (trace *#1*) or 0 mV (trace *#2*) to 120 mV.

transitions from O to C_{n+1} start to close channels again and as a result the current magnitude declines. Apparently, the state transition from O to C_{n+1} is voltage dependent and causes the current to decrease at $V_m > 130$ mV only. Such voltage dependence causes a negative slope in the steady-state current-voltage relationship (Miedema et al., 2000).

The deactivation kinetics are also in agreement with the state diagram of Fig. 3*B*. Figure 5*B* shows the deactivation kinetics of the currents in Fig. 5*A*. Remarkably, a shoulder during activation always accompanied a shoulder in the time course of deactivation (see the ''152' trace). Our interpretation is that prior to deactivation, part of the channel population occupied state C_{n+1}. Upon pulsing back to −18 mV, channels started to deactivate, i.e., state transitions started to occur in the direction of C_1 but via the open state O. The fact that the current magnitude temporarily increased indicates that despite the contribution of dO/dt (<0) caused by transitions from O to C_n, the current profile was dominated by dO/dt (>0) caused by transitions from C_{n+1} to O.

Additional evidence for an open state positioned in between two closed states came from recordings such as shown in Fig. 6. This figure shows SV currents recorded in symmetrical 100 mM K_2Malate solutions in response to a 40 or 60 mV change of V_m. Despite the *decrease* in driving force after pulsing from 140 to 100 or 80 mV, the current magnitude temporarily *increased*. Obviously, because of the symmetrical ionic conditions, such an overshoot can only be explained in terms of gating kinetics. Apparently, a 40 mV change of V_m in the negative direction evokes the same mechanism responsible for the shoulder during deactivation in Fig. 5*B*. The only difference between the two responses is that in Fig. 5*B*, with $E_K = 59$ mV, the driving force for ion flow reversed polarity after pulsing from 152 to −18 mV.

Gambale et al. (1993) studied the activation kinetics of the SV channel in radish in more detail, in particular the effect of the time in between the activating voltage pulses. When the time interval was *decreased* from 20 s to 0.3 s, the half time of activation *increased* from approximately 0.25 s to 2 s (at a V_m of 100 mV). When we employed a similar voltage pulse protocol, the *Mesembryanthemum* SV channel responded differently and this is shown in Fig. 7. Starting from a HP of 110 mV (with SV activated), the vacuole was clamped at −30 mV (to deactivate SV), first for only 0.5 s, followed by a pulse back to 110 mV. This voltage pulse protocol was repeated several times while prolonging the time at −30 mV and eventually the vacuole was clamped at −30 mV for 3.5 s. It should be noted that the deactivation of SV at −30 mV is hardly visible because the V_m of −30 mV is relatively close to E_K of −49 mV. Figure 7 shows that the shorter the time interval between two activating voltage pulses, the larger the population of SV channels that is still open at the start of the second pulse to 110 mV and the shorter the half time of SV current activation. According to Fig. 7, it takes approximately 2.5 s to completely deactivate the SV

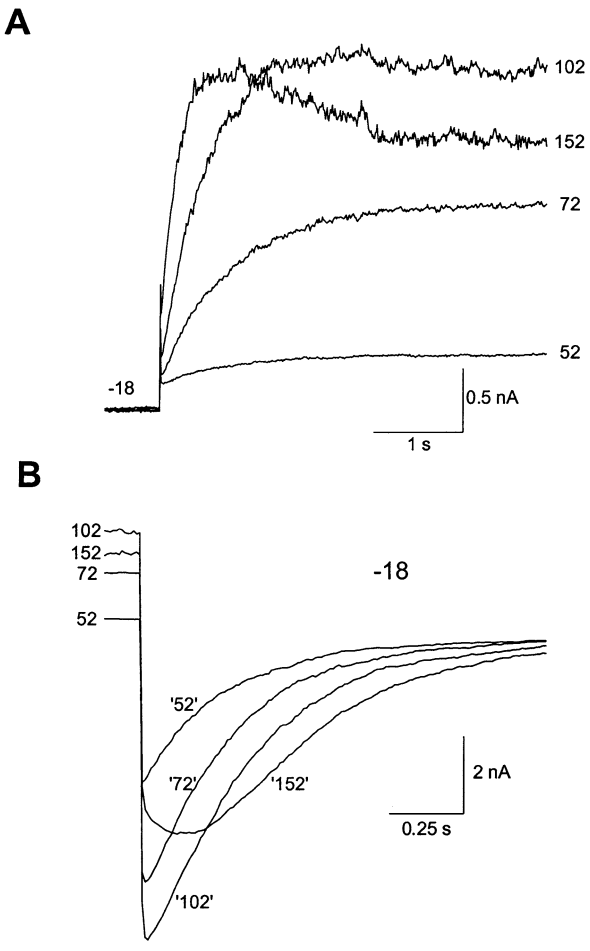

Fig. 5. Activation and deactivation of SV current. (*A*) SV current was activated after stepping V_m from an HP of −18 mV to 22–152 mV, in 10-mV steps. For reasons of clarity, traces at only four V_ms are shown. Note that approximately 1 s after activation the current recorded at 152 mV started to deactivate. The pipette and bath solution contained 160 and 10 mM K_2Malate, respectively, resulting in an E_K of 59 mV. (*B*) The deactivation kinetics of the currents shown in (*A*), recorded after pulsing back to −18 mV. Note the shoulder in the '152' trace during deactivation.

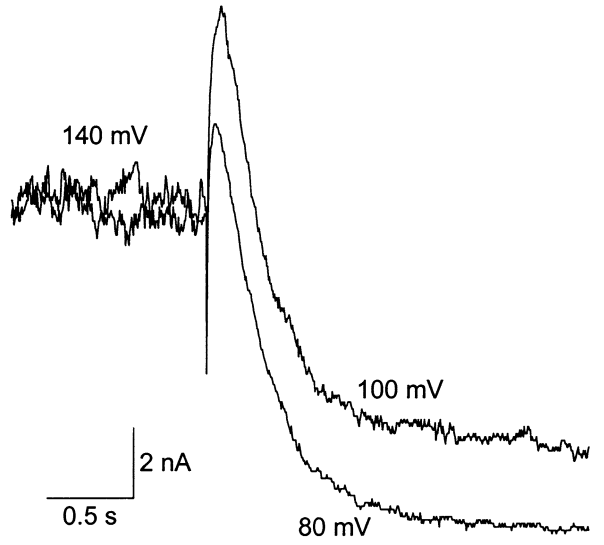

Fig. 6. Overshoots caused by small depolarizing steps of V_m. Whole-vacuole currents recorded in symmetrical 100/100 mM K_2Malate solutions. After SV current activation at 140 mV, V_m was pulsed to 80 or 100 mV. Note that the current magnitude temporarily increased after pulsing to a less depolarized potential, despite the decrease in driving force.

channel, i.e., to allow the channels to pass all the transitions back to C_1 in Fig. 3*B*.

Gambale et al. (1993) explained their results on the radish SV channel by hypothesizing a state diagram that allows transitions between C_1 and C_{n+1} in Fig. 3*B* (*see* Fig. 3*C*). Although the interpulse experiments of Fig. 7 demonstrated that the SV channel of *Mesembryanthemum* possesses kinetic characteristics other than the one in radish, we nevertheless followed Gambale et al. in their conclusion that such a cyclic state diagram can best account for the kinetic features of SV current observed experimentally. Based on the existence of such a closed loop of interconnecting states, we hypothesize that the gating kinetics of SV can best be understood in terms of the same state diagram (*see* Fig. 3*D*) that has been applied to T-type Ca^{2+} (Chen & Hess, 1990), A-type K^+ (Solc & Aldrich, 1990) and Na^+ channels (Vandenberg & Bezanilla, 1991a,b) in animal cells (Hille, 1992). It should be realized, however, that although the use of diagram of Fig. 3*D* is not without precedent and has been successfully applied to animal ion channels, the choice for this particular state diagram is more or less arbitrarly in that other kinetic schemes may give similar results. Arguments that favor a cyclic state diagram are given in the next section where the features of such kinetics are explored in more detail.

Simulations of SV Gating Kinetics

To gain a better understanding of the kinetic properties of Fig. 3*D* we also performed simulation studies (Fig. 8). State C_1 in Fig. 8*A* is printed bold, indicating that prior to the activating voltage pulse, all channels were assumed to occupy state C_1 (except for traces *#2* and 3 in Fig. 8*C*). Figure 8*A* implies that starting from C_1 there are two routes for channel activation: one in the clockwise direction and a second one in the opposite direction. The first pathway results in a relatively slow activation because prior to reaching the open state, other closed states (C_2 to C_4) have to be passed through first. In contrast, the alternative route that allows transitions directly from C_1 to O will result in a relatively fast activation. This said, the time course of activation depends on the contribution of each pathway and thus on the ratio of k_1 and k_{10}. This is demonstrated in Fig. 8*B*, which shows simulations of the different modes of SV activation kinetics, at

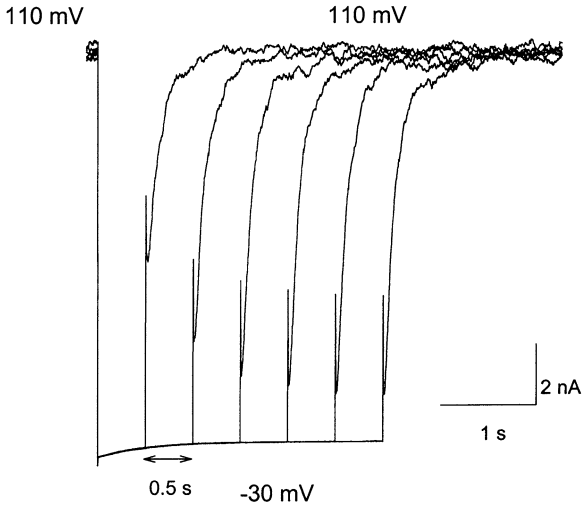

Fig. 7. Effect of the time interval between the voltage pulses on the activation kinetics. After SV current activation at 110 mV, the vacuole was clamped at a deactivating V_m of −30 mV for 0.5 s, whereupon SV was activated again at 110 mV. This procedure was repeated while the duration of the deactivation at −30 mV was prolonged by 0.5 s with each step. Whole-vacuole currents were recorded with 10 mM K_2Malate and 100 mM K_2Malate in the pipette and bath solution, respectively, resulting in an E_K of −49 mV.

potentials similar to the recordings of Fig. 5*A*. At 72 mV and with $k_1 \gg k_{10}$ ($k_{10}/k_1 = 0.02$), the time course of activation mimicked the S-shaped activation observed in Fig. 2*A*. At 152 mV and with $k_{10}/k_1 = 0.75$, the activation time course dramatically changed and now showed the typical shoulder as seen in the '152'-trace of Fig. 5*A*. These findings suggest that the value of k_{10}/k_1 is voltage sensitive and increases at more depolarized V_m. Figure 8*C* explores the appearance of the shoulder during activation a little further. This figure shows the effect of the relative degree of occupation of states C_1 and C_2 in Fig. 8*A* on the activation kinetics, with $k_{10}/k_1 = 0.75$. The shoulder is most prominent if one assumes that at the start of the activating voltage pulse all channels resided in state C_1 (trace *#1*) and disappears if one assumes that all channels occupied state C_2 (trace *#2*). With a 50/50 percent occupancy the current activation showed intermediate kinetics (trace *#3*). This figure shows that in order to see the shoulder, activation in the anticlockwise direction does not suffice. For the shoulder to appear, the majority of the channels have to initially reside in the state right next to the open state, i.e., state C_1. It should be mentioned that as far as this last conclusion is concerned, similar results were obtained with increased values of k_{10}/k_1 (*not shown*).

The kinetic scheme of Fig. 8*A* can also account for the shoulder observed during deactivation (Fig. 5*B*) and the overshoots (Fig. 6) and these simulations are shown in Figs. 8*D* and 8*E*, respectively.

Although the choice of the parameter values used for the simulations was somehow arbitrary, the cal-

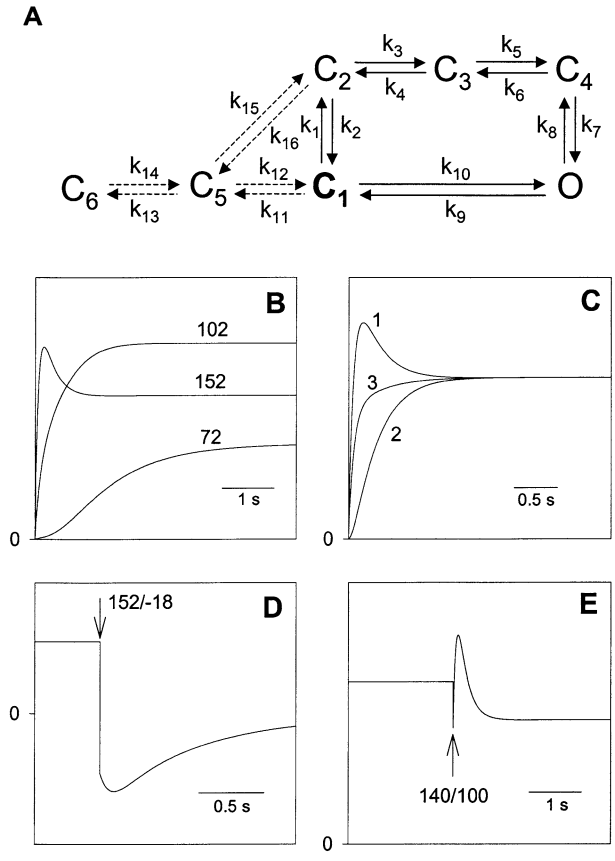

Fig. 8. Simulations of SV gating kinetics. (*A*) Cyclic state diagram that was used for the simulations. Because our main focus concerns the properties of the closed loop and in order to limit the number of parameters, transitions to and from states C_5 and C_6 were not taken into account ($k_{11} = k_{12} = k_{13} = k_{14} = k_{15} = k_{16} \approx 0\ s^{-1}$), hence the dotted arrows used for this part of the diagram. Note that by doing so, the state diagram is effectively reduced to the one of Fig. 3*C*. (*B*) Simulation of the different kinetic modes of SV activation, at 72 mV (with $k_{10}/k_1 = 0.02, k_7 = 5\ s^{-1}, k_9 = 0.4\ s^{-1}$ and $k_{10} = 0.04\ s^{-1}$); 102 mV (with $k_{10}/k_1 = 0.35, k_7 = 10\ s^{-1}, k_9 = 3\ s^{-1}$ and $k_{10} = 0.7\ s^{-1}$) and 152 mV (with $k_{10}/k_1 = 0.75, k_8 = 5\ s^{-1}, k_9 = 10\ s^{-1}$ and $k_{10} = 1.5\ s^{-1}$). E_K was assumed to be 59 mV. For comparison, *see* the experimental data presented in Fig. 5*A*. (*C*) Effect of the degree of occupancy of states and C_1 and C_2 on the activation kinetics at 152 mV and with $E_K = 59$ mV (*see* the '152' trace in (*B*)). It was assumed that initially all channels occupied either state C_1 (trace *#1*), state C_2 (trace *#2*) or, alternatively, that both states were equally occupied (trace *#3*). (*D*) Simulation of SV deactivation kinetics after stepping V_m from 152 mV to −18 mV, with $E_K = 59$ mV (*compare* with Fig. 5*B*). Parameter values at 152 mV (*see* the '152' trace in (*B*)): $k_{10}/k_1 = 0.75, k_8 = 5\ s^{-1}$, $k_9 = 10\ s^{-1}$ and $k_{10} = 1.5\ s^{-1}$. Parameter values at −18 mV: $k_{10}/k_1 = 10, k_1 = 0.002\ s^{-1}, k_7 = 5\ s^{-1}$ and $k_9 = 7\ s^{-1}$. (*E*) Simulation of an overshoot after changing V_m from 140 to 100 mV, with $E_K = 0$ mV (*see* Fig. 6). Parameter values at 140 mV: $k_{10}/k_1 = 0.75, k_8 = 5\ s^{-1}, k_9 = 10\ s^{-1}$ and $k_{10} = 1.5\ s^{-1}$. Parameter values at 100 mV: $k_{10}/k_1 = 0.35, k_7 = 10\ s^{-1}, k_9 = 12\ s^{-1}$ and $k_{10} = 0.7\ s^{-1}$. Traces in (*B–E*) show time courses of the open state (*O*), according to the state diagram in (*A*) and the equations given in Material and Methods. In order to account for effects of (changes in) driving force, values of *O* were multiplied by $(V_m - E_k)$, where E_K is the Nernst potential of K^+. Unless stated otherwise, rate constants were assigned the value of 2 s^{-1}. Except for traces *#2* and *#3* in (*C*), it was assumed that initially all channels occupied state C_1.

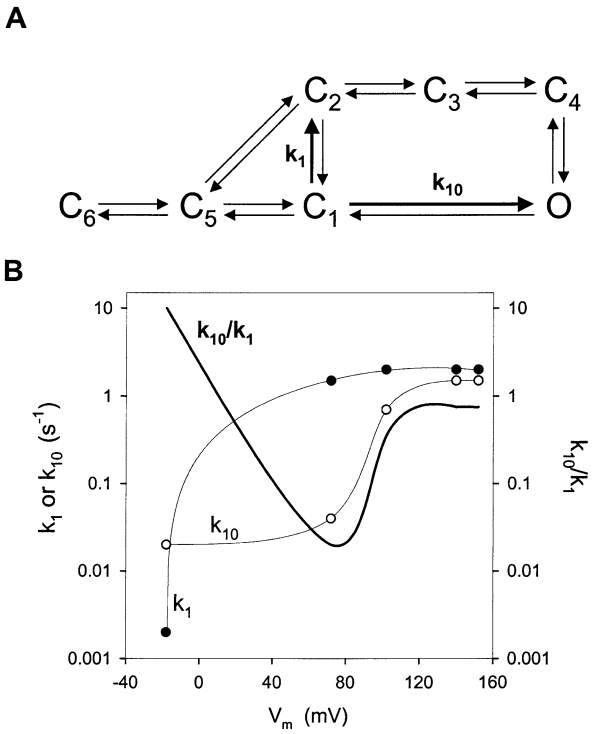

Fig. 9. Voltage dependence of rate constants k_1 and k_{10}. (*A*) State diagram of Fig. 8*A* with k_1 and k_{10} highlighted. (*B*) Plotted values of k_1 and k_{10} and their ratio (k_{10}/k_1) as used for the simulations of Fig. 8, at −18 mV, 72 mV, 102 mV, 140 mV and 152 mV.

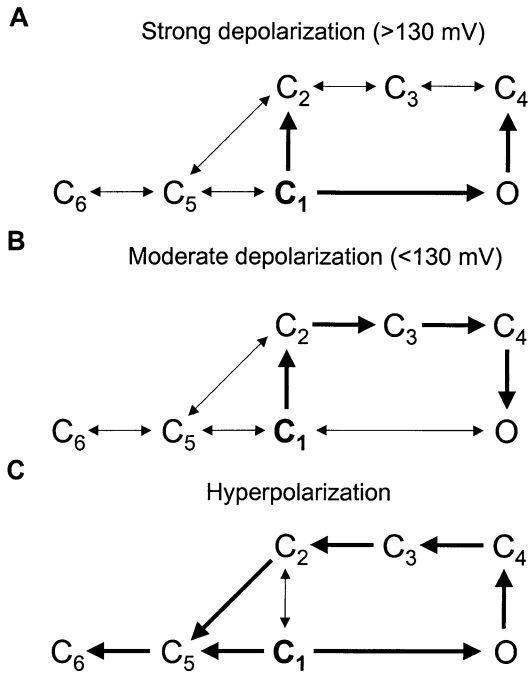

Fig. 10. Summary of the different modes of activation and deactivation discussed in this study. Starting from C_1, highlighted arrows represent the transitions that dominate the kinetics profile under that particular voltage regime (*see* Fig. 9*B*). (*A*) Transitions responsible for the fast mode of activation observed at higher depolarized potentials (>130 mV), with $k_{10}/k_1 \approx 1$. (*B*) Kinetic scheme of the S-shaped, slow mode of activation at moderate depolarization (<130 mV), with $k_1 \gg k_{10}$. (*C*) Hypothesized transitions at physiological hyperpolarization during which SV deactivates, with $k_{10}/k_1 = 10$. Along the way to C_6, part of the channel population deactivates in the anti-clockwise direction, resulting in temporary channel opening.

culations appeared to be rather sensitive to four of the ten rate constants involved, k_1 and k_{10} and to a lesser extent k_7 and k_9. Not surprisingly, three of these rate constants govern transitions directly to or from the open state. The values of k_1 and k_{10} as well as the ratio of the two (k_{10}/k_1) that were used for the simulations in Fig. 8 are plotted in Fig. 9*B*. Although both k_1 and k_{10} increase with positive-going V_m, k_1 is by far the most voltage-sensitive and increases thousandfold, from 0.002 s^{-1} at −18 mV to 2 s^{-1} at 152 mV. Note the increase of k_{10}/k_1 at both more positive and more negative V_m.

Discussion

Despite all the attention paid to the regulation of the SV channel, the controversy around SV channel functioning is still alive. The sensitivity of the SV channel to V_m seems to exclude a role for this channel in cell physiology. Magnesium sensitizes the Ca^{2+}-dependent gating of the SV channel (Pei, Ward & Schroeder, 1999) and one possibility would be that in the physiological V_m range Mg^{2+} causes SV to open (Sanders et al., 1999). Indeed, shifts of SV activation induced by elevated levels of cytosolic Mg^{2+} have been reported (Pei et al., 1999; Carpaneto, Cantù & Gambale, 2001). Although the activation kinetics shifted by as much as −60 mV, these results were observed under rather non-physiological conditions with either zero Ca^{2+} in the vacuole (Pei et al., 1999) or cytosolic Mg^{2+} and Ca^{2+} levels in the mM range (Carpaneto et al., 2001). In an attempt to identify an alternative mechanism for SV channel functioning, we approached the problem from quite a different angle and focused on the gating kinetics.

A Novel Mechanism of SV Channel Functioning?

Based on the state diagram of Fig. 8*A*, we argued that the relative values of k_1 and k_{10} determine the mode of SV activation. At modest depolarized potentials ($V_m < 130$ mV), SV activation shows the typical sigmoid-shaped time course as in Figs. 2*A* and 8*B*, indicating activation in the clockwise direction. Such activation, however, only occurs under non-physiological conditions (Fig. 2*B*). We also argued that at even less physiological V_m ($V_m > 130$ mV), SV activates predominantly along the pathway in the opposite, anti-clockwise direction. The question we

want to address here is, is it possible that under in vivo conditions, similar transitions from C_1 directly to O play a role in SV channel functioning? The data of Fig. 9*B* show that the ratio k_{10}/k_1 increases at hyperpolarized V_m, implying that even though channel opening might be unlikely at physiological V_m, if it occurs, the predominant route of SV activation is in the anti-clockwise direction, resulting in transitions from C_1 directly to O. Figure 4 demonstrates that a hyperpolarization (HP of −60 mV) prior to the activating depolarization slows down the activation kinetics. This effect of HP on the activation kinetics implies that irrespective of the temporal effect of a hyperpolarization, eventually the channel should occupy a closed state farther removed from the open state than the state it initially occupied. Therefore, suppose that initially the majority of channels occupies state C_1 in Fig. 8*A*. Upon a hyperpolarization of V_m, energized by the tonoplast-bound pyrophosphatase and/or V-type ATPase, the channel deactivates from state C_1 to C_6. Although part or even the majority of the channels may deactivate directly from C_1 to C_5 and then C_6, we hypothesize that at least a fraction of the channels deactivates in the anti-clockwise direction and via O. The novelty presented here thus is the notion that deactivation can also provoke channel opening. In a certain respect, this mechanism of channel opening is somewhat similar to the so-called reopening current observed in animal cells when Na^+ and T-type Ca^{2+} channels recover from the inactivated state (Jones, 1991; Ruppersberg et al., 1991).

If direct transitions from C_1 to O in Fig. 8*A* are indeed the route of SV channel opening at physiological V_m, it is also clear from Fig. 9*B* that opening events are expected to occur rather rarely. Although k_{10}/k_1 might increase, both rate constants decrease with negative-going V_m. In the next section, we will argue that in order to accomplish a substantial change of Ca_{cyt}, opening times of the SV channel are actually expected to be short (<1 ms). Both channel characteristics, low open probability and short opening times, which may vanish at low-pass filtering, may be the very reason in the first place that the experimental evidence for this mechanism of channel opening is still lacking.

The Impact of Ca^{2+} Influx through the SV Channel on Ca_{cyt}

Here, we will evaluate the relationship between the time the SV channel opens and the change of Ca_{cyt} upon an SV-mediated Ca^{2+} influx out of the vacuole. Due to the presence of calcium-chelating protein buffers in the cytosol, the view of an equilibrated, homogeneous Ca_{cyt} is a gross simplification. Ca^{2+} diffusion is strongly restricted and a free Ca^{2+} ion will migrate over a distance of just 0.1–0.5 μm before it chelates with a Ca^{2+}-binding protein (Clapham, 1995; Neher, 1998). In the vicinity of the mouth of open Ca^{2+}-conducting channels, the limited Ca^{2+} mobility may create microdomains of strongly elevated Ca_{cyt}. Considering their geometry with a large central vacuole and the narrow space left between the tonoplast and plasma membrane, this might be true even more for the plant cells than for animal cells. Instead of considering the entire cell volume (Allen, Sanders & Gradmann, 1998), an analysis of the Ca^{2+} influx through individual SV channels and of its strongly localized effect on Ca_{cyt} seems therefore more appropriate. For that reason, we focus on the change of Ca_{cyt} in a radius of 0.5 μm from the mouth of a single SV channel (Clapham, 1995).

The *Mesembryanthemum* SV channel has a high unitary conductance. With 160 mM K_2Malate in the pipette and 10 mM K_2Malate in the bath solution (and under symmetrical 0.3 mM free Ca^{2+}), the single-channel conductance (g) was 144 pS and the reversal potential (E_{rev}) 41 mV ($n = 4$, *data not shown*). Assuming Ohmic behavior and extrapolated to a physiological V_m of −25 mV, the single-channel current can be as high as 10 pA. First, we need an estimate of the actual Ca^{2+} flux through the channel (*see* Material and Methods). Employing a detailed kinetic analysis of SV current-voltage relationships, Allen et al. (1998) concluded that under in vivo conditions the SV current carried by K^+ is about 25 times the current carried by Ca^{2+}, implying a fractional Ca^{2+} current (FI_{Ca}) of 0.04 and an absolute Ca^{2+} current magnitude of 0.4 pA. This last value is in close agreement with current magnitudes measured in the absence of monovalent cations (Ward & Schroeder, 1994; Pottosin, Dobrovinskaya & Muñiz, 2001). Taking the 0.4 pA of Ca^{2+} current and assuming a total cytosolic Ca^{2+} buffer capacity of 99% (Sanders et al., 1999), the rate of change of Ca_{cyt} ($\Delta Ca_{cyt}/\Delta t$) in a 0.5 μm radius of the channel mouth would be as high as 600 nM/ms! Even if the absolute influx of Ca^{2+} is overestimated by a factor of ten, the rate of change of Ca_{cyt} would still be 60 nM/ms. It should also be noted that under physiological conditions, an FI_{Ca} of 0.04 indicates a P_{Ca}/P_K of approximately 0.5 (Fig. 1). This emphasizes an essential difference with most animal cation-selective channels, which are much more selective (*see also* Pottosin et al., 2001).

SV and CICR

Based on its Ca^{2+} permeability and Ca_{cyt}-sensitive gating mechanism, it was argued that the SV channel could be involved in CICR (Ward & Schroeder, 1994). Although simulation studies of SV current supported this view (Allen et al., 1998), a quantitative analysis of Pottosin et al. (1997) dismissed this possibility. The authors argued that under conditions

that favor channel opening, the driving force for Ca^{2+} ($\Delta\mu_{Ca}$) is outwardly directed (i.e., into the vacuole) rather than inwardly directed. In contrast, with V_m hyperpolarized and $\Delta\mu_{Ca} < 0$, the Ca^{2+} flux is inwardly directed (e.g., with a vacuolar and cytosolic free Ca^{2+} level of 2 mM and 100 nM, respectively, and a V_m of -50 mV, $\Delta\mu_{Ca}$ is -175 mV). In the context of our findings, SV may thus be involved in CICR after all. This would also be in agreement with, first, a study with ruthenium red which is considered to be a diagnostic tool for channels involved in CICR (Pottosin, Dobrovinskaya & Muñiz, 1999) and, secondly, a Ca^{2+}-release study employing tonoplast vesicles (Bewell et al., 1999). The $\Delta Ca_{cyt}/\Delta t$ of 600 nM/ms calculated in the previous section demonstrates that in order to achieve a localized increase of Ca_{cyt} of several hundreds of nM, the SV channel is required to be open for less than one millisecond. If SV channel gating is subject to CICR, this may cause prolonged open times. It should also be realized that the Ca^{2+}-sensitivity of SV works both ways. In the unlikely event that $\Delta\mu_{Ca}$ is outwardly directed, the Ca^{2+}-dependent gating mechanism of SV will promote channel closure, thereby preventing any further loss of Ca_{cyt}. In other words, if the flux of Ca^{2+} through the SV channel reverses, the mechanism responsible for CICR turns into a safety valve for Ca_{cyt}.

Conclusion

As pointed out by Hille (1992), simulations and data fitting cannot prove a particular gating model, at best they can discount certain alternatives. With this in mind, we nevertheless argue in favor of the same state diagram that has been applied to a number of cation-selective ion channels in animal cells. Our findings are summarized in Fig. 10. The state diagram of Fig. 10 allows current activation along two pathways. So far, all research focused on the activation at non-physiological V_m in the clockwise direction, i.e., starting from C_1 to C_2, C_3 and C_4, eventually to O (Fig. 10*B*). Here, we provide evidence for the existence of an alternative route of channel activation directly from C_1 to O, a pathway more profound at stronger depolarizations (Fig. 10*A*). A challenging idea is that under physiological conditions, V_m hyperpolarization also evokes transitions from C_1 directly to O, followed by transitions to C_4 and eventually all the way to C_6. The presumptions underlying our hypothesis are, first, that at resting V_m (-50 to 0 mV) the channel predominantly occupies state C_1 in Fig. 8*A*. Secondly, the final result of a deactivating V_m hyperpolarization is that more channels are forced to occupy a closed state farther removed from the open state than C_1. During this process and on its way to state C_6 in Fig. 8*A*, (part of) the channel population may temporarily visit the open state. In a way, the mechanism of SV activation at hyperpolarized V_m proposed here is the mirror image of the mechanism of channel activation at depolarized V_m. In the first case with V_m hyperpolarized, the channel open probability is low, but it is commonly believed that V_m is hyperpolarized. In contrast, in the latter case with V_m depolarized, the channel open probability is relatively high but chances that V_m actually enters this voltage range are pretty slim. Obviously, both modes of activation do not mutually exclude each other and it might well be possible that both mechanisms complement each other and play their own specific role in SV channel functioning.

This study was supported by Grants awarded to O.P. by CONACyT (4745-N) and DGAPA (IN-202000).

References

Allen, G.J., Sanders, D., Gradmann, D. 1998. Calcium-potassium selectivity: kinetic analysis of current-voltage relationships of the open, slowly-activated channel in the vacuolar membrane of *Vicia faba* guard-cell. *Planta* **204:**528–541

Allen, G.J., Sanders, D. 1997. Vacuolar ion channels in higher plants. In: The Plant Vacuole. R.A. Leigh and D. Sanders, Eds. pp. 217–252. Academic Press, Inc. London

Barkla, B.J., Vera-Estrella, R., Maldonado-Gama, M., Pantoja, O. 1999. ABA induction of vacuolar H^+-ATPase activity in *Mesembryanthemum crystallinum* L. is developmentally regulated. *Plant Physiol.* **120:**811–819

Bertl A., Blumwald, E., Coronado, R., Eisenberg, R., Findlay, G., Gradmann, D., Hille, B., Köhler, K., Kolb, H.A., MacRobbie, E., Meissner, G., Miller, C., Neher, E., Palade, P., Pantoja, O., Sanders, D., Schroeder, J., Slayman, C., Spanswick, R., Walker, A., Williams, E. 1992. Electrical measurements on endomembranes. *Science* **258:**873–874

Bewell, M.A., Maathuis, F.J.M., Allen, G.J., Sanders, D. 1999. Calcium-induced calcium release mediated by a voltage-activated cation channel in vacuolar vesicles from red beet. *FEBS Letters* **458:**41–44

Carpaneto, A., Cantù, A.M., Gambale, F. 1999. Redox agents regulate ion channel activity in vacuoles from higher plant cells. *FEBS Letters* **442:**129–132

Carpaneto, A., Cantù, A.M., Gambale, F. 2001. Effects of cytoplasmic Mg^{2+} on slowly activating channels in isolated vacuoles of *Beta vulgaris*. *Planta* **213:**457–468

Chen, C., Hess, P. 1990. Mechanism of gating of T-type calcium channels. *J. Gen. Physiol.* **96:**603–630

Clapham, D.E. 1995. Calcium signaling. *Cell* **80:**259–268

Gambale, F., Cantù, A.M., Carpaneto, A., Keller, B.U. 1993. Fast and slow activation of voltage-dependent ion channels in radish vacuoles. *Biophys. J.* **65:**1837–1843

Hedrich, R., Neher, E. 1987. Cytoplasmic calcium regulates voltage dependent ion channels in plant vacuoles. *Nature* **329:**833–835

Hille, B. 1992. Ionic Channels of Excitable Membranes. Sinauer Associates, Massachusetts

Johannes, E., Brosnan, J.M., Sanders, D. 1992. Parallel pathways for intracellular Ca^{2+} release from the vacuole of higher plant. *Plant J.* **2:**97–102

Jones, S.W. 1991. Not an open-and-shut case. *Nature* **353:**603–604

Miedema, H., Balderas, E., Pantoja, O. 2000. Current oscillations under voltage clamp conditions: an interplay of negative slope conductance and series resistance. *J. Membrane Biol.* **173:**31–37

Miedema, H., Pantoja, O. 2001. Anion modulation of the slow-vacuolar channel. *J. Membrane Biol.* **183:**137–145

Neher, E. 1998. Usefulness and limitations of linear approximations to the understanding of Ca^{2+} signals. *Cell Calcium* **24:**345–357

Pantoja, O., Gelli, A., Blumwald, E. 1992. Voltage-dependent calcium channels in plant vacuoles. *Science* **255:**1567–1570

Pei, Z.-M., Ward, J.M., Schroeder, J.I. 1999. Magnesium sensitizes slow vacuolar channels to physiological cytosolic calcium and inhibits fast vacuolar channels in *Fava* bean guard cell vacuoles. *Plant Physiol.* **121:**977–986

Pottosin, I.I., Tikhonova, L.I., Hedrich, R., Schönknecht, G. 1997. Slowly activating vacuolar channels can not mediate Ca^{2+}-induced Ca^{2+}-release. *Plant J.* **12:**1387–1398

Pottosin, I.I., Dobrovinskaya, O.R., Muñiz, J. 1999. Cooperative block of the plant endomembrane ion channel by ruthenium red. *Biophys. J.* **77:**1973–1979

Pottosin, I.I., Dobrovinskaya, O.R., Muñiz, J. 2001. Conduction of monovalent and divalent cations in the Slow Vacuolar channel. *J. Membrane Biol.* **181:**55–65

Robinson, R.A., Stokes, R.H. 1965. Electrolyte Solutions. Butterworths, London

Ruppersberg, J.P., Frank, R., Pongs, O., Stocker, M. 1991. Cloned neuronal I_K(A) channels reopen during recovery from inactivation. *Nature* **353:**657–660

Sanders, D., Brownlee, C., Harper, J.F. 1999. Communicating with calcium. *Plant Cell* **11:**691–706

Schneggenburger, R., Zhou, Z., Neher, E. 1993. Fractional contribution of calcium to the cation current through glutamate receptor channels. *Neuron* **11:**133–143

Sole, C.K., Aldrich, R.W. 1990. Gating of single non-*shaker* A-type potassium channels in larval *Drosophila* neurons. *J. Gen. Physiol.* **96:**135–165

Vandenberg, C.A., Bezanilla, F. 1991a. Single channel, macroscopic, and gating currents from sodium channels in the squid giant axon. *Biophys. J.* **60:**1499–1510

Vandenberg, C.A., Bezanilla, F. 1991b. A sodium channel gating model based on single channel, macroscopic ionic, and gating currents in the squid giant axon. *Biophys. J.* **60:**1511–1533

Voit, E.O. 2000. Computational Analysis of Biochemical Systems. Cambridge University Press, UK

Ward, J.M., Schroeder, J.I. 1994. Calcium-activated K^+ channels and calcium-induced calcium release by slow vacuolar ion channels in guard cell vacuoles implicated in the control of stomatal closure. *Plant Cell* **6:**669–683

Wijngaard, van den, P.W.J., Bunney, T.D., Roobeek, I., Schönknecht, G., De Boer, A.H. 2001. Slow vacuolar channels from barley mesophyll cells are regulated by 14-3-3 proteins. *FEBS Letters* **488:**100–104